First-Principles Study on Rutile TiO_2 Quantum Dots

Haowei Peng, Jingbo Li,* Shu-Shen Li, and Jian-Bai Xia

State Key Laboratory for Superlattices and Microstructures, Institute of Semiconductors, Chinese Academy of Sciences, P.O. Box 912, Beijing 100083, People's Republic of China

Received: May 14, 2008; Revised Manuscript Received: June 22, 2008

The electronic structure of rutile TiO_2 quantum dots (QDs) are investigated via the first-principles band structure method. We first propose a model to passivate the rutile TiO_2 surfaces for the local density approximation calculations. In this model pseudohydrogen atoms are used to passivate the surface dangling bonds, which remove the localized in-gap surface states in the TiO_2 QDs. As the size of the QD decreases, the band gap evolves as $E_g(\text{dot}) = E_g(\text{bulk}) + 73.70/d^{1.93}$, where E_g(dot) and d are the band gap and diameter of the QD, and E_g(bulk) is the band gap of the bulk rutile TiO_2. The valence band maximum and the conduction band minimum states of the QDs are distributed mostly in the interior of the QDs, and they well inherit the atomic characteristics of those states of the bulk rutile TiO_2.

1. Introduction

TiO_2 is an important material in both the energy and environmental applications, ranging from photovoltaics and photocatalysis to photo/electrocgromics and sensors.[1] Most of these applications are based on the properties of TiO_2 as an efficient and environmentally benign semiconductor photocatalyst. The photocatalytic activity of a semiconductor photocatalyst largely depends on three factors: (1) the light absorption properties, (2) the reduction and oxidation rates on the surface by the electrons and holes, (3) and the electron−hole recombination rate. As the size of the material decreases, the specific surface area and surface-to-volume ratio increase dramatically. This should be beneficial to many TiO_2-based devices, because most of the reactions happen on the surfaces. However, as the size decreases, the quantum confinement effect and the surface states become very important, as well as the shape effect. The particle size also impacts the phase stability,[2] which is a critical parameter determining the suitability for special applications. To improve the photocatalytic performance under visible light irradiation, metal- and nonmetal-doped TiO_2 nanomaterials have been studied.[1] People also try to control the surface states of TiO_2 nanoparticles using organic ligands to modifying the surfaces.[3] Theoretically, Baicker et al. performed a molecular dynamics simulations to investigate structural properties of TiO_2 quantum dots (QDs), for example, the Ti−O bond length as a function of dot size, phase, and temperature, and its dependence on the coordination environment of the Ti atom.[4] Barnard and Zapol investigated the effects of particle morphology and surface hydrogenation on the stability of TiO_2, where they studied several hydrogen surface passivation schemes.[5] Later on, they modeled some anatase nanoparticles and studied their structures and electronic properties using a self-consistent tight-binding method,[6] but they cannot obtain the relation between the quantum-confinement energies, $\Delta E_g = E_g(\text{dot}) - E_g(\text{bulk})$, and the diameters of the QDs. The characteristics of the valence band maximum (VBM) and the conduction band minimum (CBM) for the QDs are not yet understood clearly. To prompt the development and improve the qualities of related devices, we need to know these properties of the TiO_2 QDs.

To acquire this knowledge, we can turn to the first-principles calculation method, which has been successively applied to the studies of Si QDs,[7] III−V and II−VI QDs,[8] and some core/shell QDs. [9] Comparing with other approaches such as $k\cdot p$ effective mass method and empirical tight-binding method, the first-principle method is free of empirical parameters and more reliable. In this paper, we have studied the properties mentioned above for the rutile TiO_2 QDs using the first-principles band structure method.

A common problem in studying the electronic structure of the QDs is the surface passivation. Experimentally, large organic molecules are often used to passivate the QD surface.[3] Due to their complexity, it is difficult to calculate such structures. Fortunately, a simple atomistic passivation method is available,[8,10] where pseudohydrogen atoms ^{Z}H, which have a fractional nuclear charge Z and a corresponding fractional electron charge, are used to terminate the dangling bonds. For 4-fold coordinated systems, a $Z = (8 - m)/4$ psudo-hydrogen atom well terminates a dangling bond of a surface atom with formal valence charge m.[8] Recently, the suitability of this method was confirmed in the calculations of the IV, III−V, and II−VI nanostructures. [11] As to rutile TiO_2, the structure is a bit more complex than those of the diamond, zinc blende, and wurtzite structures, so the surface passivation needs a special scheme, which will be discussed at length in the following sections.

The rest of the paper is organized as follows. Section 2 describes the calculation details and the passivation method. In section 3, we present the evolution of the band gap of the rutile TiO_2 QDs, and compare the electronic structure of the QDs and that of the bulk rutile TiO_2. The effects of the passivation are also presented in Section 3. Finally, a brief summary of this paper is given in Section 4.

2. Method

In this study, the total energy calculations are performed with the local density approximation (LDA) based on the density functional theory (DFT), as implemented in the Vienna ab initio simulation package (VASP).[12] The projector augmented wave method (PAW)[13] is chosen to represent the ionic potentials. In

* To whom correspondence should be addressed. E-mail: jbli@semi.ac.cn.

10.1021/jp8042973 CCC: $40.75
Published on Web 08/15/2008

TABLE 1: The Calculated Structural Parameters of Rutile TiO_2, Compared with the Experimental[15] Results

	this work	experimental
a (Å)	4.568	4.5936
c (Å)	2.926	2.9587
c/a	0.641	0.6441
u	0.305	0.3048

all the calculations, the convergency of the total energy with respect to the plane-wave bases kinetic-energy cutoff and k-sampling is checked to be within 0.001 eV, and all structures have been relaxed until the Hellmann−Feynman force is less than 0.05 eV/Å. The Monkhorst−Pack method[14] is used to sample the Brillouin zone. A $12 \times 12 \times 12$ k-grid is used for the bulk unit cell calculation, and only the Γ-point is used for the QD calculations. The LDA optimized parameters of the bulk rutile TiO_2 are in good agreement with the experiments,[15] as shown in Table 1. Next we will use these parameters to model the QDs.

The modeling of the QDs is quite direct. First, we build the bare (unpassivated) QDs. Fixing a Ti atom at the center, we remove all the atoms outside of the sphere with a radius r. Then the surface Ti atoms with more than two dangling bonds and the surface O atoms with more than one dangling bonds are also removed, according to a previous molecular dynamics simulations.[4] In this study, we calculate three TiO_2 QDs which contain 79, 245, and 587 atoms, respectively (not including the passivating atoms). All the QDs are surrounded by the (001), (110), and (111) faces of the rutile structure. Then we use the pseudohydrogen atoms to passivate the surface. The nuclear charge Z of the pseudohydrogen atoms are determined by a simple chemical consideration of the covalent bond, similar as the case of 4-fold coordinated systems. However, we need to remember that the Ti−O bond itself has a characteristic of strong ionic bonding.[16] In the rutile structure, Ti atom is coordinated by six O atoms which form a slightly distorted octahedron, and the O atom is coordinated by three titanium atoms in a plane. In this ionic system, each Ti contributes two thirds electrons to each O atom, so that the O has the stable eight-electron closed-shell electron configuration. Therefore, to passivate the O dangling bond we use the $Z = 2/3$ pseudohydrogen ($^{2/3}$H) atoms, while the $Z = 4/3$ pseudohydrogen ($^{4/3}$H) atoms are chosen to terminate the surface Ti dangling bonds, since two electrons are needed to satisfy the Ti−$^{4/3}$H bond. The Ti−$^{4/3}$H and O−$^{2/3}$H bond lengths are extracted from two model calculations. We model an octahedral Ti($^{4/3}$H)$_6$ cluster and a regular triangular O($^{2/3}$H)$_3$ cluster. The LDA calculated bond lengths of the Ti−$^{4/3}$H bond and O−$^{2/3}$H bond are 1.728 and 1.012 Å, respectively. In the rutile structure, the LDA optimized bond length of the apical Ti−O bond is 1.972 Å, while that of the equatorial one is 1.924 Å. Last, we put the passivated QDs in a supercell, where the QDs are surrounded by a 10 Å thick vacuum layer to ignore the unphysical interactions. In Figure 1, we show all the seven possible surface configurations in this study. During the relaxation, the surface Ti−O bonds become shorter; however, the bond-lengths between the surface Ti, O atoms, and the corresponding pseudohydrogen atoms are almost unchanged.

Before studying the rutile TiO_2 QDs, we have checked the availability of the surface passivation method on some TiO_2 flat surfaces. We choose four crystal faces of the rutile structure, (001), (100), (110), (111). For each face, we build a slab with 7−10 atom layers, and the surface dangling bonds are terminated by corresponding pseudohydrogen atoms. A 10 Å thick vacuum layer is also added in the confined dimension, and a corresponding two-dimensional Monkhorst-Pack k-grid[14] is used to sampling the Brillouin zone. Generally speaking, there are two criteria about the availability of the passivation method. On the one hand, due to the quantum confinement effect, the band gap of the slab or dot is larger than that of the bulk; on the other hand, with all the dangling bonds passivated, the in-gap states arising from the dangling bonds should be removed. For all the four slabs, if the dangling bonds are not terminated, the Ti dangling bonds introduce defect levels near the CBM, while the O dangling bonds introduce defect levels near the VBM. After passivation, the in-gap states for all the four slabs are removed, and the energy band gaps of the (001), (100), (110), (111) slabs are 1.84, 1.98, 1.97, and 2.32 eV, respectively, which are larger than the band gap of the bulk rutile TiO_2, 1.68 eV. That is to say, the passivation method satisfies the two criteria. The effects of the passivation on the QD will be discussed particularly in Section 3.3.

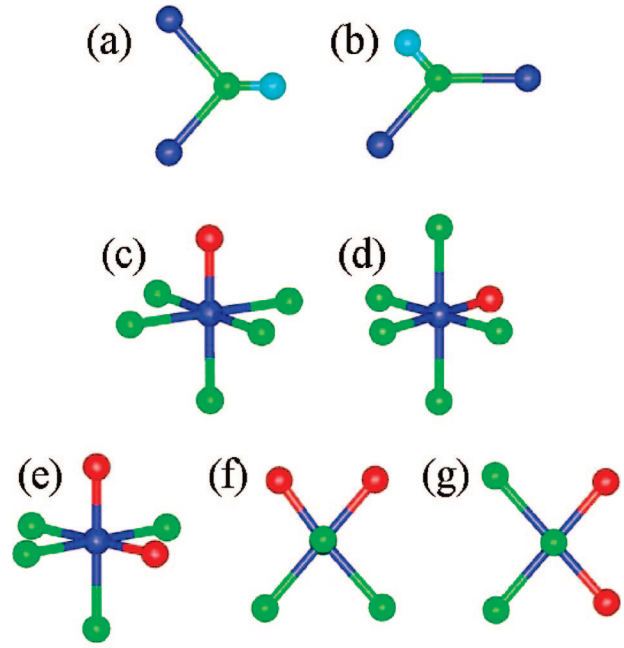

Figure 1. All the possible passivating configurations in this study. The blue, green, skyblue, and red balls represent Ti atoms, O atoms, $^{2/3}$H, and $^{4/3}$H pseudohydrogen atoms, respectively. (The color scheme is kept for all the figures in the paper.) In (a,b), one apical and one equatorial O dangling bond is passivated, respectively. In (c,d), one apical and one equatorial Ti dangling bond is passivated, respectively. In (e), one apical and one equatorial Ti dangling bonds are passivated. In (f,g) in the top view, two equatorial Ti dangling bonds are passivated, but the angles between the dangling bonds are 81.70 and 99.30°, respectively.

3. Results and Discussion

3.1. Bulk Rutile TiO_2. For comparison, we briefly summarize here the electronic structure of the bulk rutile TiO_2. Rutile TiO_2 has a direct band gap at Γ-point. The LDA calculated band gap is 1.68 eV, which is much smaller than the experimental value[17] of 3.0 eV due to the well-known LDA error. The calculated total density of states (DOS) and projected DOS for the bulk rutile TiO_2 are shown in Figure 2. The basic structure unit in the rutile TiO_2 is the distorted TiO_6 octahedron. From the DOS patterns, we know (1) the lower part of the valence band is composed of the σ-bonding states arising from the coupling between the Ti-3d and O-2p orbitals; (2) the top of the valence band is mainly composed of the nonbonding O-2p_π

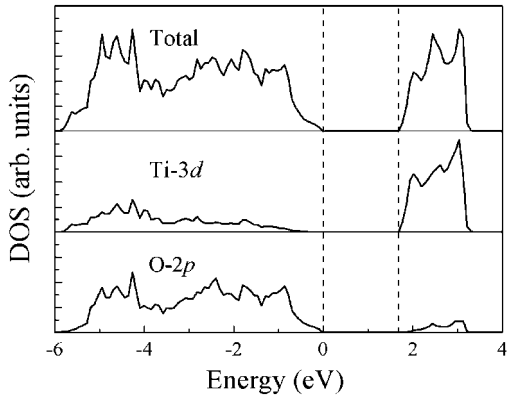

Figure 2. The total and projected densities of states (DOS) for the bulk rutile TiO_2. The two vertical dotted lines indicate the energy positions of the VBM and the CBM, respectively.

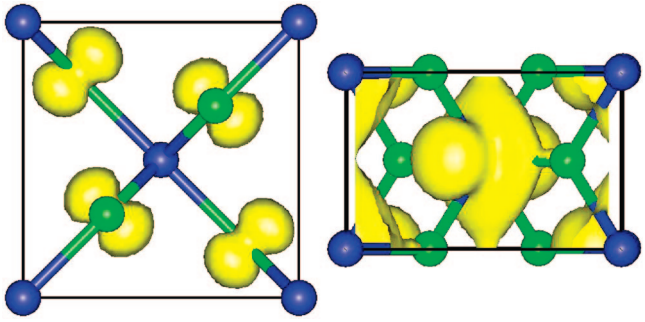

Figure 3. The wave function square contour plots of the VBM (left) and CBM (right) for the bulk rutile TiO_2. For clarity, we choose the top view and the front view for the VBM and CBM plots, respectively.

TABLE 2: The Numbers of the 4-, 5-, and 6-Coordinated Ti Atoms and 2-, 3-Coordinated O Atoms in the 79-, 245-, and 587-Atom Rutile TiO_2 QDs[a]

dots	Ti(4)	Ti(5)	Ti(6)	O(2)	O(3)
79	14	8	5	30	22
245	22	26	33	76	78
587	40	48	107	134	258

[a] The numbers in the bracket indicate the coordination number.

orbitals (out of the Ti_3O plane); (3) the conduction band mainly consists of the Ti-3d orbtals; and (4) the bottom of the conduction band is mainly composed of Ti-3d t_{2g} orbitals which coupled with each other slightly. In the rutile structure, the Ti−Ti distance is a little shorter than that in the anatase structure. So the coupling in the rutile structure between the 3d t_{2g} orbitals near the CBM is stronger than that in the anatase structure.[18] In Figure 3, we plot the wave function square contours of the VBM and CBM states, where the characteristics of the O-2p_π and Ti-3d t_{2g} orbitals are clearly shown as mentioned above.

3.2. Rutile TiO_2 QDs. In this study, we calculate three QDs, $Ti_{27}O_{52}(^{4/3}H)_{36}(^{2/3}H)_{30}$, $Ti_{81}O_{164}(^{4/3}H)_{70}(^{2/3}H)_{76}$, and $Ti_{195}O_{392}(^{4/3}H)_{128}(^{2/3}H)_{134}$. Excluding the pseudohydrogen atoms, they have 79, 245, and 587 atoms, respectively. In Table 2, we show the numbers of the 4, 5, and 6-coordinated Ti atoms and 2, 3-coordinated O atoms in the three QDs. The larger the QD is, the smaller is the proportion of the under-coordinated atoms, as the surface-to-volume ratio decreases. All the three QDs take a near-sphere shape and are not stoichiometric. So we estimate the effective sizes by $d = [3a^2c\cdot(2n_{Ti} + n_O)/4\pi]^{1/3}$, where a and c are the LDA optimized lattice constants of rutile TiO_2 listed in Table 1, n_{Ti} is the number of the Ti atoms in the QDs, and n_O is the number of the O atoms in the QDs. This gives the effective sizes $d = 11.56$, 16.80, and 22.50 Å for the QDs with 79, 245, and 587 atoms, respectively. Comparing the structures before and after relaxation, the QDs contract a little. While on the surface, most of the Ti atoms move inward by about 0.05 Å, and most of the O atoms move outward by about 0.02 Å. The bond lengths between the surface Ti and O atoms are in good agreement with previous molecular dynamic calculations.[4] The most probable bond lengths between the 4-coordinated Ti and 2-coordinated O atoms are about 1.865 Å, and the most probable bond lengths between the 5-coordinated Ti and 2-coordinated O atoms are about 1.910 Å.

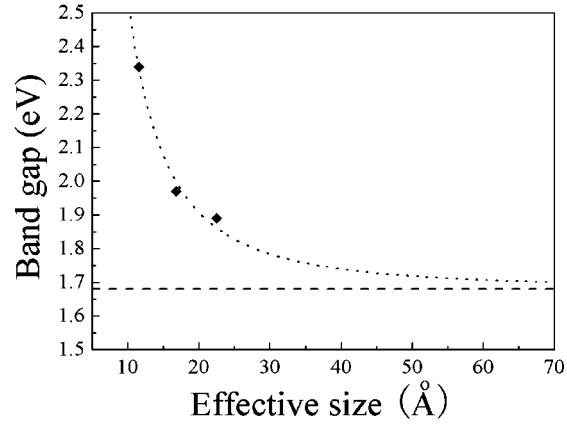

Figure 4. The calculated band gap for rutile TiO_2 QDs with different sizes. The horizontal dashed line indicates the LDA energy band gap of the bulk rutile TiO_2. The dotted line is the fitted curve $E_g(\text{dot}) = E_g(\text{bulk}) + 73.70/d^{1.93}$.

As the size decreases, the energy gap of the QD becomes larger and larger, due to the quantum confinement effect. In Figure 4, the calculated LDA band gaps for the three QDs are shown as a function of the effective size. The difference between the band gap of the QDs and that of the bulk, ΔE_g, are fitted according to the expression $\Delta E_g = \beta/d^\alpha$, where d is the effective size of the QDs. The analytic fitting results in $\alpha = 1.93$ and $\beta = 73.70$ that seems to follow the $1/d^2$ scaling according to the effective-mass model, while for the III−V and II−VI QDs the values of α are between 1.0 and 1.3, and 1.6 for the Si QDs, according to the previous first-principles calculations.[19] In recent experimental work,[20] the size of the rutile QDs is successfully controlled, and the quantum confinement effect is studied. The diameter of two rutile QDs is 1.47 and 1.70 nm based on the TEM data, and their band gap change based on the optical waveguide spectra is 0.55 and 0.34 eV, respectively. Using our fitted functions, we obtain the band gap change 0.51 and 0.30 eV for the two QDs, respectively, showing good agreement.

In order to investigate the nature of the VBM and CBM states of the QDs, we have calculated the wave function squares of the near-edge states for the fully passivated QDs. In Figure 5, we plot the wave function square contours of the VBM state and the state exactly below the VBM (VBM-1) for the 245-atom QD from three different perspectives. Those of the state exactly above the CBM (CBM + 1) and the CBM state are shown in Figure 6. First, we notice that there is almost no distribution on the surface passivating pseudohydrogen atoms. This means that the passivation works well for the TiO_2 dots. Second, the wave functions of the VBM and CBM states are distributed mostly in the interior of the dot, especially the CBM state. This agrees with the previous studies on Si QDs,[7] InP quantum wires, and CdSe QDs.[19] Third, comparing the left pattern in Figure 1 and the top right pattern in Figure 5, we

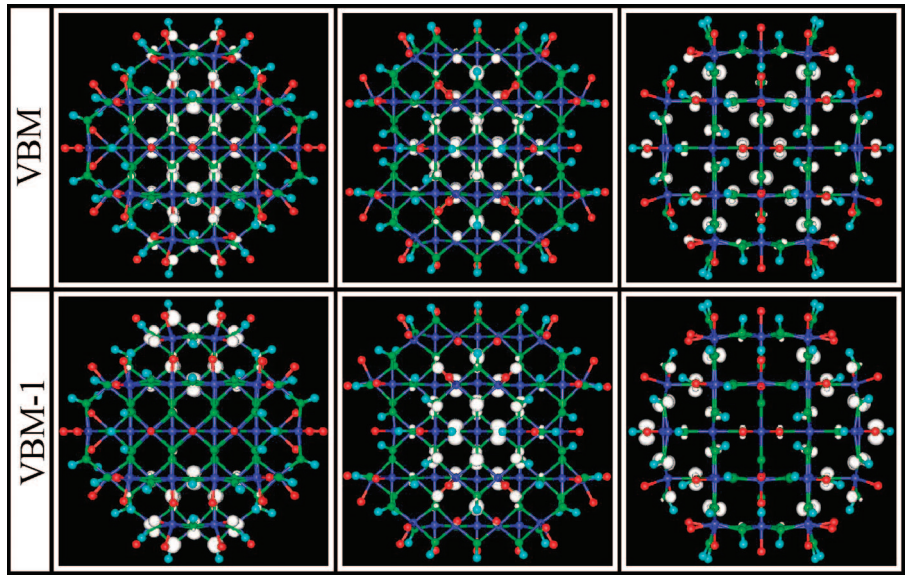

Figure 5. The wave function square contour plots of the VBM state and the state exactly below the VBM (VBM − 1) for the 245 atom rutile TiO_2 QD. The three columns from left to right are the views from the (110), (100), and (001) directions, respectively.

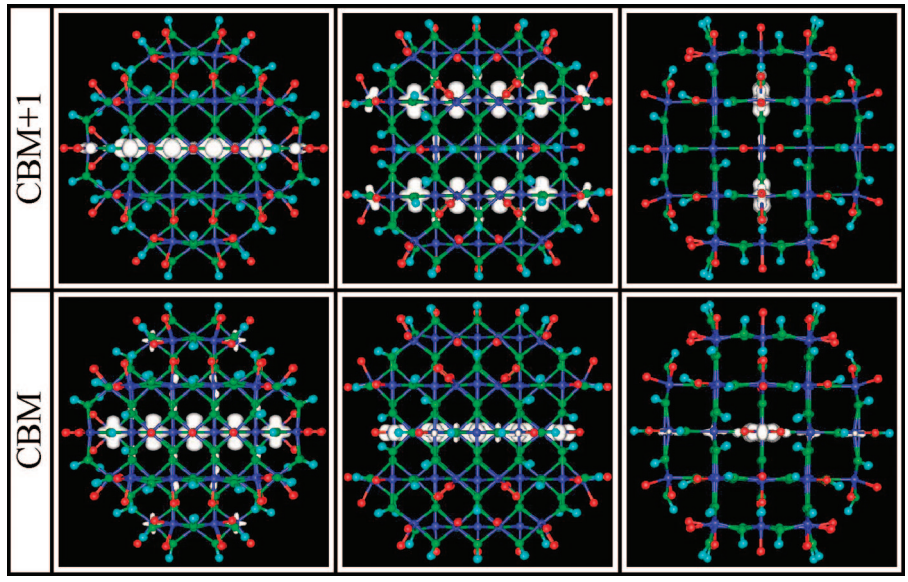

Figure 6. The same as in Figure 5 but for the state exactly above the CBM (CBM + 1) and the CBM state.

find that both the VBM states of the rutile TiO_2 bulk and QD have the same characteristic of O-2p_π orbitals. Similarly, the CBM and CBM + 1 states of the QD have the characteristic of Ti-3d t_{2g} orbitals, as show in Figure 6. In other words, the VBM and CBM states in the QDs inherit well the atomic characteristics of those states in the bulk rutile TiO_2.

3.3. Effects of the Passivation on the Rutile TiO_2 QDs. To illustrate the effects of the passivation, we carry out a series of comparative studies on the small 79-atom QD. In Figure 7, we plot the calculated DOS for the fully passivated 79 atom QD. The LDA energy band gap is 2.34 eV, and there is no surface state in the gap. The CBM and VBM states are similar to those of the 245-atom QD, as shown in Figure 5 and Figure 6, respectively.

For comparison purpose, we study another three 79-atom QDs: one with both the Ti and O dangling bonds unpassivated, one with the Ti dangling bonds unpassivated, and one with the O dangling bonds unpassivated. The DOS for these QDs are shown in Figure 8a−c, respectively, where the surface states are marked out by arrows, and their wave function square

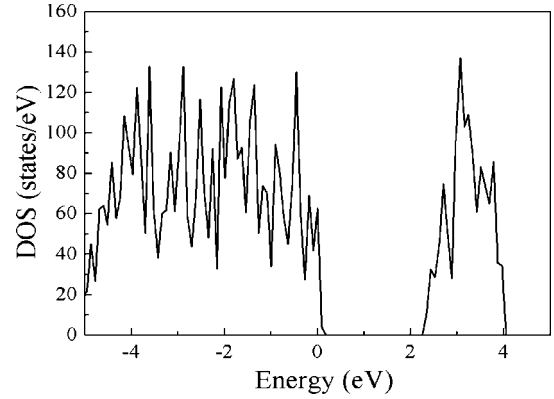

Figure 7. The DOS for the fully passivated 79 atom rutile TiO_2 QD. The Fermi energy is at the zero energy.

contours are plotted on the right of the DOS patterns. For the bare QD, during the relaxation, the surface is reconstructed. In the band gap, there is a peak of localized surface states. Most of these surface states are distributed on the surface Ti dangling

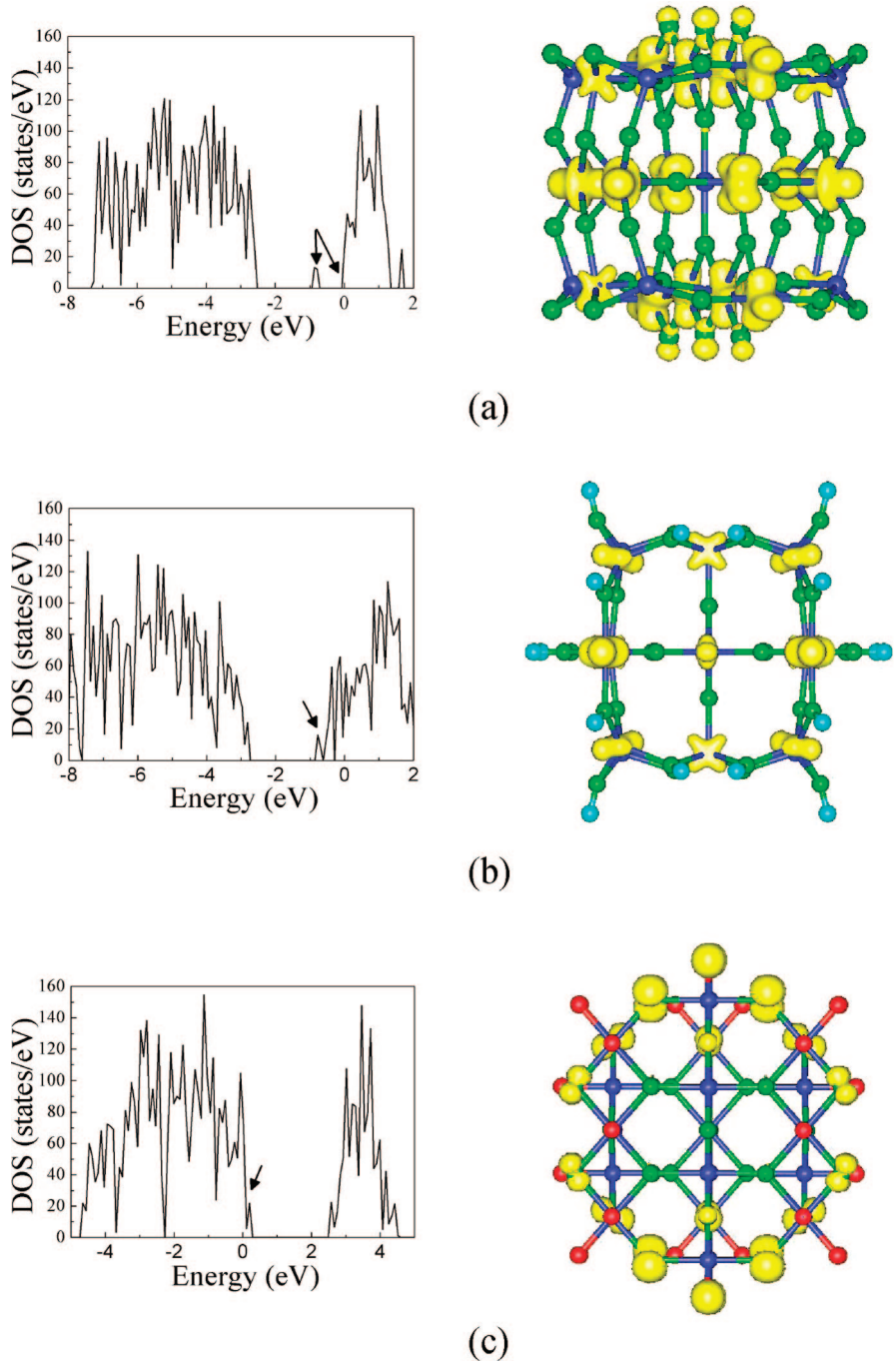

Figure 8. The DOSs for (a) the bare QD, (b) the QD with unpassivated Ti dangling bonds, and (c) the QD with unpassivated O dangling bonds. The Fermi energy is at the zero energy. For each QD, the surface states are marked out with arrow, and the corresponding wave function square contours are plotted on the right. To clearly illustrate the characteristics of the surface states, different views are chosen for the three plots.

bonds, and a small proportion of the states are distributed on the top and bottom O dangling bonds according to Figure 8a. When the O dangling bonds are passivated, the Ti dangling bonds act as donor defects, which induce a great many of surface states near the CBM. According the contours plot in Figure 8b, the surface states are mainly located at the surface Ti sites, while on the oxygen sites there is no distribution. When only the Ti dangling bonds are passivated, near the VBM there are surface states arising from the O dangling bonds, as shown in Figure 8c. The O dangling bonds act as acceptor defects.

From the comparison, we find that the passivation removes the surface states from the energy gap or near the gap edge while leaving the VBM and CBM states unchanged. This enables us to conclude that the passivation scheme described in Section 2 works well for the TiO_2 materials. And we believe that our passivating method is useful for investigating the properties of the TiO_2 nanomaterials, especially the optical properties that relate closely to many applications of the TiO_2 nanomaterials.

4. Summary

In this paper, the electronic structure of the rutile TiO_2 quantum dot is studied using the first-principles band-structure method. Pseudohydrogen atoms are used to passivate the surface dangling bonds. The availability of the passivation method is checked on both flat surfaces and quantum dot surfaces. The passivation successively removes the surface states in or near

the energy gap. As the size decreases, the evolution of the band gap increases as $\Delta E_g = 73.70/d^{1.93}$. The fitting results are in good agreement with previous experiments. The VBM and the CBM states of the quantum dots are distributed mostly in the interior of the dots, and they have the similar atomic characteristics of those states of the bulk rutile TiO_2.

Acknowledgment. J.L. gratefully acknowledges financial support from "One-hundred Talents Plan" of the Chinese Academy of Sciences. This work was supported by the National Natural Science Foundation of China under Grants 60521001 and 60776061.

References and Notes

(1) Chen, X.; Mao, S. S. *Chem. Rev.* **2007**, *107*, 2891.
(2) Zhang, H.; Banfield, J. F. *J. Phys. Chem. B* **2000**, *104*, 3481.
(3) de la Garza, L.; Saponjic, Z. V.; Dimitrijevic, N. M.; Thurnauer, M. C.; Rajh, T. *J. Phys. Chem. B* **2006**, *110*, 680.
(4) Naicker, P. K.; Cummings, P. T.; Zhang, H.; Banfield, J. F. *J. Phys. Chem. B* **2005**, *109*, 15243.
(5) Barnard, A. S.; Zapol, P. *Phys. Rev. B* **2004**, *70*, 235403.
(6) Barnard, A. S.; Zapol, P. *Phys. Rev. B* **2004**, *73*, 205405.
(7) Wang, L. W.; Li, J. *J. Phys. Chem.* **1994**, *98*, 2158.
(8) Wang, L. W.; Li, J. *Phys. Rev. B* **2004**, *69*, 153302.
(9) Wang, L. W.; Li, J. *Appl. Phys. Lett.* **2004**, *84*, 3648.
(10) Shiraishi, K. *J. Phys. Soc. Jpn.* **1990**, *59*, 3455.
(11) Huang, X.; Lindgren, E.; Chelikowsky, R. *Phys. Rev. B* **2005**, *71*, 165328.
(12) Kresse, G.; Joubert, D. *Mater. Sci.* **1996**, *6*, 15.
(13) Kresse, G.; Joubert, D. *Phys. Rev. B* **1999**, *59*, 1758.
(14) Monkhorst, H. J.; Pack, J. D. *Phys. Rev. B* **1976**, *13*, 5188.
(15) Abarahams, S. C.; Bernstein, J. L. *J. Chem. Phys.* **1971**, *55*, 3206.
(16) Grant, F. A. *Rev. Mod. Phys.* **1959**, *31*, 646.
(17) Pascual, J.; Camassel, J.; Mathieu, H. *Phys. Rev. Lett.* **1977**, *39*, 1490.
(18) Peng, H.; Li, J.; Li, S. S.; Xia, J. B. *J. Phys.: Condens. Matter* **2008**, *20*, 125207.
(19) (a) Li, J.; Wang, L. W. *Chem. Mater.* **2004**, *16*, 4012. (b) Li, J.; Wang, L. W. *Phys. Rev. B* **2005**, *72*, 125325.
(20) Satoh, N.; Nakashima, T.; Kamikura, K.; Yamamoto, K. *Nat. Nanotechnol.* **2008**, *3*, 106.

JP8042973